Accepted Manuscript

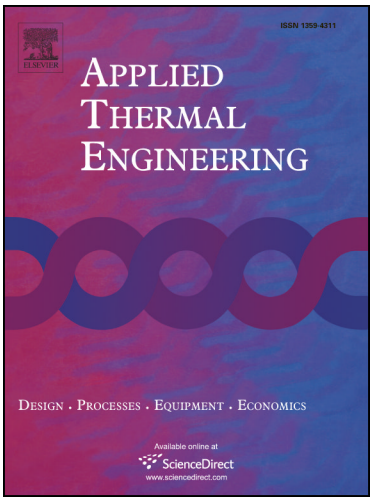

Effect of non-condensable gas on the behaviours of a controllable loop thermosyphon under active control

Jingyu Cao, Gang Pei, Michele Bottarelli, Chuxiong Chen, Dongsheng Jiao, Jing Li

PII: S1359-4311(18)30765-8
DOI: https://doi.org/10.1016/j.applthermaleng.2018.09.132
Reference: ATE 12741

To appear in: *Applied Thermal Engineering*

Received Date: 2 February 2018
Revised Date: 26 August 2018
Accepted Date: 28 September 2018

Please cite this article as: J. Cao, G. Pei, M. Bottarelli, C. Chen, D. Jiao, J. Li, Effect of non-condensable gas on the behaviours of a controllable loop thermosyphon under active control, *Applied Thermal Engineering* (2018), doi: https://doi.org/10.1016/j.applthermaleng.2018.09.132

This is a PDF file of an unedited manuscript that has been accepted for publication. As a service to our customers we are providing this early version of the manuscript. The manuscript will undergo copyediting, typesetting, and review of the resulting proof before it is published in its final form. Please note that during the production process errors may be discovered which could affect the content, and all legal disclaimers that apply to the journal pertain.

Effect of non-condensable gas on the behaviours of a controllable loop thermosyphon under active control

Jingyu Cao[a], Gang Pei*[a], Michele Bottarelli[b], Chuxiong Chen[a], Dongsheng Jiao[a], Jing Li[a]

[a] *Department of Thermal Science and Energy Engineering, University of Science and Technology of China, Hefei 230027, China*

[b] *Department of Architecture, University of Ferrara, via Quartieri 8, 44121 Ferrara, Italy*

*Corresponding author. Tel.: 0551-63607367; fax: 0551 63603742.

E-mail address: peigang@ustc.edu.cn

Abstract

Controllable loop thermosyphon (CLT) can be used as a significant temperature management component in solar- and electric-powered cool-storage refrigerators. However, the behaviours of CLT with non-condensable gas (NCG) under active control require further investigation. In this study, air is mixed in working fluid R134a as NCG to evaluate the steady-state and start-stop performances of CLT for selected control modes. CLT with 0% to 0.62% NCG is tested. The larger the amount of NCG is, the lower the heat transfer rate is. When the mass ratio of NCG reaches 0.62%, the steady-state heat transfer rate varies from 245.0 W to the minimum 118.6 W for different heat sink temperatures. This finding means that CLT loses efficacy due to the excess NCG. In addition, the start-up performances of the two modes decrease as the mass ratio of NCG increases to 0.31% and become entirely unacceptable when NCG reaches 0.47%. By contrast, the stopping time of CLT remains less than 100 s in various conditions. Results indicate that the mass ratio of NCG should be less than 0.47%, and CLT with NCG is suggested to be controlled by the valve in the vapour line.

Keywords: *loop thermosyphon, refrigerator, non-condensable gas, start-stop*

1. Introduction

Two-phase heat transfer devices, such as heat pipes, capillary pumped loops, loop heat pipes, and thermosyphons, are reliable, highly effective, compact, and cost-effective and thus widely used in heat transfer. With technological advancement, the application of such devices in several crucial

fields, including temperature management for microelectronic components and nuclear reactors and renewable energy, has been explored [1-3]. Extensive research has been conducted to verify further the reliability of these devices under new backgrounds. Research results demonstrate that non-condensable gas (NCG) is one of the most common causes of performance degradation [4-11]. NCG is a gaseous substance that remains in the gas state during the condensation procedure in two-phase heat transfer devices. It is generally caused by (a) the combination of residual gases, such as air, and working fluids that appear in the charging procedure; (b) a leak in negative-pressure operation; and (c) chemical reactions among working fluids, impurities, and structural materials [12-13]. NCG commonly accumulates in the condenser section of two-phase heat transfer devices; thus, the overall heat transfer capacity decreases with the heat transfer area of the condenser [14, 15].

Among two-phase heat transfer devices, the loop thermosyphon or separate heat pipe possesses advantages in cost and heat transfer limit. Many studies have been conducted recently in this popular field. Tong et al. investigated the self-regulating performance of an R744 loop thermosyphon and revealed the interaction between two parallel evaporators [16]. Ziapour et al. designed a mini tube loop thermosyphon solar water heater for a photovoltaic/thermal (PV/T) system. The loop thermosyphon increased the solar cells' packing factor and the thermal efficiency of the passive PV/T solar system [17]. Mameli et al. designed a novel multi-evaporator loop thermosyphon whose transfer capability was five times larger than that of previous technologies [18]. Zhang et al. studied the two-phase stratified flow boiling of water in a loop thermosyphon with a horizontal evaporator. Periodic transition of the flow pattern and different types of dynamic instabilities were observed during the visualized investigation [19]. Panse et al. proposed a loop thermosyphon with an open microchannel manifold and focused on the flow boiling procedure. The loop thermosyphon with a small ethanol head of 0.2 m reached the heat flux of 136 W/cm^2 [20]. Louahlia-Gualous et al. proposed new correlations for the heat transfer coefficients of the evaporator and condenser of loop thermosyphons. The results indicated that micro-porous layers help increase the heat transfer surface

in the evaporator, and the thermal resistance of the evaporator is reduced by 25% under the effect of a thin porous layer [21]. Zhang et al. proposed microchannel parallel-flow heat exchangers for a loop thermosyphon to cool data centers. Simulation results showed that the optimal filling ratio is 150% because no superheating or sub-cooling occurs [22].

New application backgrounds, structures, and operating modes have resulted in a high demand for CLT with long lifespan and high reliability. However, studies on the effects of NCG on loop thermosyphons are limited. Dube et al. studied the impact of NCG on the behaviours of loop thermosyphon heat exchangers. Their results showed that NCG decreases the thermal conductance of loop thermosyphons, and the adverse effects are pronounced at low temperatures [23]. Toyoda et al. developed a loop thermosyphon for cooling electronic devices. The study discovered that the adverse impact of NCG is mainly reflected in the degradation of condensing performance [24]. He et al. further investigated the effect of NCG on the steady-state operation of a loop thermosyphon and focused on its start-up behaviour. The results showed that the presence of NCG leads to an increase in operating temperature and that the effect of NCG is significantly correlated with the operating temperature range of the loop thermosyphon. The study also confirmed that NCG prolongs the starting time and increases the liquid superheat and temperature overshoot [25, 26]. Recently, Huang et al. studied the start-up behaviour of a loop thermosyphon and used a gas-liquid separator. A rapid increase in system pressure was observed during start-up because the vapour block area retarded the vapour transmission from the evaporator to the condenser during start-up [27]. Battaglia et al. introduced a cooling technology for power electronics based on a loop thermosyphon. The research showed that NCG can adversely affect cooling performance, but the reservoir structure helps avoid this problem [28]. These existing studies mainly focus on the effects of NCG on the performance of passive heat transfer, but they are insufficient.

In our previous paper, we proposed a controllable loop thermosyphon (CLT) that can be used as a temperature management component in solar- and electric-powered cool-storage refrigerators [29-31].

The heat transfer in CLT can be stopped and started at a high frequency to manage the loading temperature. Although preliminary study shows that the performance of a properly working CLT meets the standard requirements of refrigerators, further reliability study on temperature management capability is necessary, given significant improvements in the efficiency and temperature accuracy of refrigerators. In the current study, we therefore emphasize the effect of NCG not only on steady-state performance but also on start-up and stopping behaviours. CLTs with and without NCG are tested in a steady heat transfer state. Then, the start-up and stopping behaviours under two control modes are examined. Tests are conducted with different amounts of NCG and at varying heat sink and heat source temperatures.

2. Experimental setup and charging procedure

The CLT prototype is depicted in Fig. 1. The CLT is made up of copper tubes. The evaporator and condenser are designed with tube-in-tube helical heat exchangers, and heat is transferred from the heat source to the heat sink by the working fluid of CLT in the counter-flow heat transfer mode. Valves 1 and 2 are installed in the vapour and liquid lines, respectively. The inner diameter of the CLT is 10 mm, and that of the shells in the evaporator and condenser is 23 mm. The lengths of the liquid line, vapour line, evaporator, and condenser are 1500, 1300, 1340, and 1340 mm, respectively. The CLT and test system are covered with a thermal insulating layer, which is made of a rubber foam insulation material, and are located in a thermostatic chamber, as shown in Fig. 2. The thermal conductivity of the rubber foam insulation material is 0.034 W/m·k at 0 ℃. The insulation thicknesses for the water cycle, glycol solution, and CLT are 9, 19, and 37 mm, respectively. The heat sink temperature of CLT, which is affected by the inlet temperature and flow rate of the glycol solution, is regulated by the cold bath DC-3015. The heat source temperature is controlled by the hot bath DC-0515. The temperature adjustment ranges of DC-0515 and DC-3015 are −5 ℃-100 ℃ and −30 ℃-100 ℃, respectively. The control accuracy reaches 0.5 ℃.

Temperature and pressure sensors are installed at the inlet and outlet of the heat exchange

section to directly monitor the status of the working fluid in CLT. The temperature differences and volume flow rates in the ethylene glycol solution and water are measured with flow meters and temperature sensors. The measurement points are shown in Fig. 1, and data are collected with the Agilent 34970 data acquisition system every 5 s. Table 1 presents the detailed information.

A 2TGH-1C vacuum pump is used for charging in this experiment, and the ultimate vacuum reaches 0.003 Pa. R134a (204 g) is filled into the CLT as the working fluid, and different quantities of air are mixed into it to serve as NCG. The detailed charging procedure is as follows. First, pure R134a is filled into then extracted from CLT for several times to completely clean the residual air adsorbed on the surface of the copper tube. Second, to test CLT without NCG, 204 g R134a is directly filled into CLT. Lastly, to test CLT with different ratios of NCG, the vacuum valve is slightly opened to inhale a small amount of air before filling 204 g R134a. The charge quantity of air is directly related to the inner pressure of CLT before filling R134a according to the following equation.

$$M_{NCG} = \rho_{NCG}(P,T)V_{CLT} \quad , \tag{1}$$

where V_{CLT} is the volume of CLT and M_{NCG} and ρ_{NCG} are the mass and density of NCG, respectively.

The partial pressure of NCG can be obtained when CLT remains in the equilibrium state after filling R134a.

$$P_{NCG} = P - P_{GR}(T)\,, \tag{2}$$

where P_{NCG} is the partial pressure of NCG, P is the inner gas pressure of CLT, and P_{GR} is the partial pressure of gaseous R134a.

Then, the mass ratio of NCG in the gas region under normal charging temperature (20 °C) can be evaluated.

$$\begin{aligned} X_{NCG} &= \frac{M_{NCG}}{M_{NCG}+M_{GR}} \times 100\% \\ &= \frac{\rho_{NCG}(T,P_{NCG})}{\rho_{NCG}(T,P_{NCG})+\rho_{GR}(T,P_{NCG})} \times 100\% \end{aligned} \quad , \tag{3}$$

where X_{NCG} is the mass ratio of NCG in the gas region and M_{GR} and ρ_{GR} are the mass and density of gaseous R134a, respectively. ρ_{NCG} and ρ_{GR} can be calculated with the software REFPROP 7.0 on the basis of the measured pressure and normal charging temperature.

3. Experimental methods and calculation

Considering the background of refrigerators, the constant stopping status of CLT should be clearly described. The water and glycol solution stably flow even when the valves are closed for a long time. In this case, the heat transfer rate of CLT is 0 W, and the pressure is constant.

The start-up and stopping of CLT are based on the two control valves. During start-up and stopping processes, the flow of water and glycol solution remains stable. Two effective control modes are selected to start/stop the flow of the working fluids: (i) turn on/off valve 1 when valve 2 remains open and (ii) simultaneously turn on/off valves 1 and 2.

For convenience, normal test conditions are adopted unless mentioned otherwise. Ambient temperature, which is controlled by the thermostatic chamber, is approximately 20 °C. The inlet temperature and flow rate of water are 5 °C and 100 L/h, respectively. The inlet temperature and flow rate of the glycol solution are −25 °C and 80 L/h, respectively. On this basis, CLT is measured under different inlet temperatures of the glycol solution $T_{g,in}$, inlet water temperatures $T_{w,in}$, and amounts of NCG. Different amounts of NCG, namely, 0, 11.6, 23.2, 34.8, and 46.4 mg, are mixed in R134a; that is, X_{NCG} varies from 0% to 0.62%. $T_{g,in}$ varies from −25 °C to −17 °C, and $T_{\mathrm{w,in}}$ is regulated from 5 °C to 9 °C. CLT is tested in a steady condition and two selected active control modes. The start-up, stopping, and steady-state performances of CLT are investigated in detail.

The heat transfer rate of the CLT is a key parameter and should be calculated at any time to evaluate the heat transfer behaviours of the CLT. Considering the good heat-insulating property of the heat insulation layer, the heat transfer rate in the evaporator is calculated as a representative.

$$Q = \rho_w \dot{V}_w C_w (T_{w,in} - T_{w,out}), \tag{4}$$

where Q is the heat transfer rate of CLT; ρ_w, $\dot{V}_w$, and C_w are the density, volume flow rate, and

specific heat capacity of water, respectively; and $T_{w,in}$ and $T_{w,out}$ are the inlet and outlet water temperatures, respectively.

Table 1 shows the uncertainties of the independent variables. On this basis, the uncertainty of the dependent variable can be obtained by applying the theory of error propagation [31, 32]. In this study, the uncertainty of the steady-state heat transfer rate of CLT is evaluated as 10.8%.

4. Results and discussion

4.1 Effect of NCG on steady-state behaviour

Steady-state experiments are performed while the mass ratio of NCG X_{NCG} increases from 0% to 0.62% and the temperature of the inlet glycol solution $T_{g,in}$ varies from −25 °C to −17 °C. Figure 3 shows the average heat transfer rate of CLT in the steady state for different X_{NCG} values. For the $T_{g,in}$ of −25 °C, the steady-state heat transfer rate of CLT decreases from 380.6 W to 245.0 W while X_{NCG} increases. The heat transfer decrement trend remains stable even when $T_{g,in}$ varies; the more NCG exists, the lower the heat transfer capability of CLT is. However, a difference can be observed from the impact of $T_{g,in}$ when X_{NCG} increases from 0.47% to 0.62%. For X_{NCG} of 0.47%, the heat transfer rate is 300.8 W when $T_{g,in}$ is −25 °C, and it decreases to 216.1 W when $T_{g,in}$ rises to −17 °C. The reduced ratio is approximately 71.8%. For X_{NCG} of 0.62%, the heat transfer rate is 245.0 W when $T_{g,in}$ is −25 °C, and it sharply decreases to the minimum of 118.6 W when $T_{g,in}$ rises to −17 °C. The reduced ratio is lower than 50%. Considering the application background of cool-storage refrigerators, the steady-state heat transfer rate of CLT is within an acceptable range when X_{NCG} is within 0% to 0.47%. However, when X_{NCG} reaches 0.62%, CLT cannot retain sufficient heat transfer capability as the heat sink temperature increases [33-35]. Therefore, CLT with 0.62% NCG can be deemed to lose efficacy. The following analysis and study on the start-stop behaviours of CLT only focus on the X_{NCG} range of 0% to 0.47%.

The adverse effect of NCG on heat transfer can be analyzed as follows. Most of the NCG cannot be dissolved in the liquid R134a and mainly exists in the vapour space. When CLT operates

stably, the pressure in the evaporator is normally higher than that in the condenser. Therefore, NCG accumulates in the forepart of the condenser, occupies the heat transfer area between R134a and the glycol solution, decreases the condensation heat transfer efficiency, and increases the flow resistance of R134a. This effect can be reflected by the difference between the average evaporator and condenser pressures, ΔP, and the temperature difference between the inlet and outlet R134a in the evaporator (ΔT). In this study, ΔP is affected by the following factors: (1) existence of NCG, (2) curving structure of CLT, and (3) pressure drop caused by the control valves and sight glasses. ΔP and ΔT are calculated as follows:

$$\Delta P = \frac{P_{e,in} + P_{e,out}}{2} - \frac{P_{c,in} + P_{c,out}}{2} \quad , \tag{4}$$

$$\Delta T = T_{e,out} - T_{e,in} \quad , \tag{5}$$

where $P_{c,in}$, $P_{c,out}$, $P_{e,in}$, and $P_{e,out}$ are the pressures at the condenser inlet, condenser outlet, evaporator inlet, and evaporator outlet of CLT, respectively; $T_{e,in}$ and $T_{e,out}$ are the inlet and outlet R134a temperatures of the evaporator, respectively.

Figure 4 shows that with increasing X_{NCG}, ΔT and ΔP increase from 11.1 °C to 14.7 °C and from 3 kPa to 5.5 kPa, respectively. The increasing ΔP shows that the phase-transition temperature of the condenser gradually deviates from that of the evaporator under the effect of NCG. Correspondingly, heat transfer reduction appears in the evaporator. The degrees of inlet undercooling and outlet overheat of the evaporator, which are reflected by ΔT, increase with the amount of NCG. This phenomenon shows that the existence of NCG in CLT causes a deviation from the optimum operating condition, and this adverse effect increases with the amount of NCG.

4.2 Effect of NCG on start-up performance

The start-up procedure of CLT is different from that of a normal loop thermosyphon due to its special stopping status. Considering the application background of refrigerators, the CLT has to start up quickly and reach the maximum heat transfer state as soon as possible to provide enough cold

energy to the fresh food compartment when the users open the thermal insulating door and the temperature of the fresh food compartment rises sharply. Therefore, the start-up performance of the CLT in this paper is closely related to its capability to quickly reach the steady heat transfer status with the maximum heat transfer rate. The start-up time is adopted as the key parameter to evaluate the start-up performance of the CLT and it is defined as the time consumed to reach the steady heat transfer state with the maximum heat transfer rate, which allows for a 5% margin of error.

Previous studies have shown that CLTs can start up in 25 s, and start-up behaviours remain stable even when the heat sink temperature and structure vary [30]. In the current study, we test the start-up behaviour in modes I and II under different X_{NCG}. Given a $T_{g,in}$ of –25 °C, the start-up procedures of CLT with different amounts of NCG in mode I are shown in Fig. 5. The start-up time overall increases with X_{NCG}. The start-up time for CLT without NCG is approximately 25 s, and the heat transfer variation in the start-up procedure remains stable when a small amount of NCG is filled into CLT. However, when X_{NCG} increases to 0.47%, the start-up time increases to 55 s. Specifically, heat transfer deterioration appears and is maintained for about 200 s when X_{NCG} reaches 0.47%. Therefore, the start-up time of CLT with 0.47% NCG significantly increases to 245 s. Fig. 6 shows the start-up procedures in mode II. A similar phenomenon appears, and the time consumed to restore normal heat transfer becomes longer when X_{NCG} is 0.47%. The heat transfer rates in the periods of heat transfer deterioration are less than 200 W. We speculate that the minimum value can further decrease with the heat sink temperature.

In modes I and II, the start-up procedures of CLT with 0.47% NCG are similar and can be analyzed together. The relatively high heat transfer rate that appears at the beginning of the start-up procedure is mainly caused by sensible heat transfer. The temperature of liquid R134a in the liquid line is much lower than the inlet water temperature. Therefore, a transient high heat transfer rate appears when the liquid R134a flows into the evaporator with the assistance of gravity. Heat transfer deterioration can be analyzed as follows. When CLT is completely stopped, NCG exists in the upper

part of the vapour line and condenser. This distribution is relatively uniform even when the pressure and temperature of the condenser part are lower than those of the vapour line. If excessive NCG exists in CLT, this evenly distributed gas can block the condensation heat transfer and increase the flow resistance in the vapour line during start-up process. Then, under the effect of pressure difference and a period of two-phase flow, NCG will accumulate again in the forepart of the condenser, and the heat transfer of CLT will finally increase.

To further test the start-up performance of CLT with NCG, $T_{g,in}$ is increased from −25 °C to −17 °C. Table 2 shows the average start-up time under different test conditions. The start-up time in the two modes remains stable when X_{NCG} is less than 0.16%, whereas it increases remarkably with $T_{g,in}$ when X_{NCG} is higher than 0.31%. When X_{NCG} is 0.47% and $T_{g,in}$ is −17 °C, the heat transfer rate of CLT only increases to 70% of the steady-state heat transfer rate in 30 min during the start-up test in both modes. The heat transfer of CLT remains relatively stable most of the time and cannot automatically return to normal during this period. This phenomenon can be regarded as a start-up failure. In addition, the experiments show good repeatability when the start-up time is less than 300 s. However, the start-up time becomes unstable when it is higher than 300 s, and the repeated experiments show that the fluctuation range is normally within 60 s. These behaviours confirm that heat transfer deterioration only appears when the amount of NCG reaches 0.47%. NCG needs more time to accumulate in the forepart of the condenser, and the pressure difference and flow rate of R134a decrease with increasing $T_{g,in}$. Thus, heat transfer deterioration can be maintained for a long time when the temperature difference between the evaporator and condenser is small.

The difference in the start-up performance of the two control modes is mainly reflected by the average start-up time of CLT. Table 2 shows that the start-up performance of CLT in mode I is similar to that in mode II when X_{NCG} is lower than 0.31%. However, the average start-up time of mode II under different $T_{g,in}$ values becomes much longer than that of mode I when X_{NCG} increases to 0.47%. To compare the start-up behaviours of the two control modes further, CLT with 0.47% NCG

is tested under different heat sink and heat source temperatures. On the basis of normal test conditions, $T_{g,in}$ and $T_{w,in}$ are adjusted, and the behaviours of modes I and II in three typical operating conditions are compared. The three operating conditions are as follows: (1) $T_{g,in}$ is −25 °C and $T_{w,in}$ is 5 °C, namely, normal test conditions; (2) $T_{g,in}$ is −21 °C and $T_{w,in}$ is 7 °C; and (3) $T_{g,in}$ and $T_{w,in}$ are −17 °C and 9 °C, respectively. Fig. 7 shows that the average start-up time of both modes increases as the temperature range of CLT rises. The average start-up time of mode I remains lower than that of mode II in all three operating conditions. The results further demonstrate that the start-up performance of mode I is relatively better than that of mode II when X_{NCG} increases to 0.47%.

Generally, a small quantity of NCG has a limited impact on the start-up behaviours of modes I and II. However, the start-up performance of both modes decreases when X_{NCG} increases to 0.31% and becomes entirely unacceptable when X_{NCG} reaches 0.47%. When CLT is affected by NCG, the overall start-up performance of mode I is better than that of mode II.

4.3 Effect of NCG on stopping performance

To evaluate the effects of NCG on the stopping behaviours of modes I and II, comparative experiments are performed with $T_{g,in}$ being −25 °C. Fig. 8 shows the stopping procedures. The following phenomena are observed. The decreasing trends of heat transfer become rapid as X_{NCG} increases in the two modes. In mode I, the time required to reach a constant stopping status, which allows for a 5% margin of error, decreases from 95 s to 65 s as X_{NCG} increases from 0% to 0.47%. In mode II, this stopping time also decreases from 85 s to 50 s. The stopping performance of mode II is considered better than that of mode I because the stopping time of mode II is shorter than that of mode I for different X_{NCG} values, but the gap is not evident.

Residual heat transfer exists in the stopping procedure because the phase-transition temperature of R134a in the evaporator of an operating CLT is lower than that of a stopping CLT. This temperature is nearly equal to the inlet temperature of water. The degree of this temperature increase directly affects the amount of residual heat transfer in the evaporator. Considering that the

phase-transition temperature is closer to the inlet temperature of water as the heat transfer rate of CLT decreases, the stopping time decreases with increasing X_{NCG}. $T_{g,in}$ varies from −25 °C to −17 °C, and further tests are performed to verify the aforementioned analysis. Figure 9 shows that even when $T_{g,in}$ and X_{NCG} vary, the stopping time of CLT with different amounts of NCG remains lower than 100 s. The experiment results follow the aforementioned laws. Given $T_{g,in}$, the stopping time generally decreases when a large amount of NCG exists in CLT. Thus, the stopping performance of CLT improves with the existence of NCG when its amount is less than 0.47%.

5. Conclusions

In this study, a test rig was set up to analyze the impact of NCG on the behaviours of CLT under active control. To evaluate the steady-state and start-stop behaviours of the two selected control modes, comparative tests were conducted by varying the amount of NCG and the heat sink and heat source temperatures. The following conclusions were derived.

1. Given the $T_{g,in}$ of −25 °C, the steady-state heat transfer rate of CLT decreases from 380.6 W to 245.0 W when X_{NCG} increases from 0% to 0.62%. The minimum heat transfer rate reaches 118.6 W when X_{NCG} increases to 0.62% and $T_{g,in}$ decreases to −17 °C. The difference between the average evaporator and condenser pressures and the temperature difference between the inlet and outlet R134a in the evaporator increase with NCG. The steady-state tests showed that the existence of NCG in CLT can cause a deviation from the optimum operating condition. Thus, the heat transfer rate decreases with increasing X_{NCG}. The overall heat transfer capability is acceptable when X_{NCG} is within 0% to 0.47%.

2. In the start-up procedures of modes I and II, heat transfer deterioration appears with increasing X_{NCG} and decreasing $T_{g,in}$. During this period of heat transfer deterioration, the heat transfer capability of CLT maintains approximately 70% of the steady-state heat transfer, thus increasing the start-up time. When X_{NCG} is less than 0.16%, the start-up time remains stable within 15 s to 30 s, whereas it significantly increases with $T_{g,in}$ when X_{NCG} is higher than 0.31%. Start-up

failures appear in both modes when X_{NCG} is 0.47% and $T_{g,in}$ is −17 °C, and the heat transfer of CLT cannot automatically return to normal within 30 min. The results showed that the adverse effect of NCG on the start-up performance of CLT is negligible when X_{NCG} is less than 0.16% and becomes entirely unacceptable when X_{NCG} reaches 0.47%. Moreover, the overall start-up performance of mode I is relatively better than that of mode II under the effect of NCG.

3. The stopping time of modes I and II remains lower than 100 s when X_{NCG} and $T_{g,in}$ vary from 0% to 0.47% and from −25 °C to −17 °C, respectively. The stopping time generally decreases with increasing X_{NCG} and $T_{g,in}$. Therefore, the stopping performance of CLT improves with the existence of NCG when its amount is less than 0.47%. The stopping performance of mode II is better than that of mode I, although the advantage is insignificant.

In general, considering that the rapid heat transfer start-up capability of CLT plays a crucial role in improving the temperature control accuracy of novel cool-storage refrigerators, NCG, which is mixed into the working fluid during the charging and operating procedures of CLT, should be less than 0.47%. In addition, CLT with NCG is suggested to be controlled by mode I. Given that start-up performance degradation considerably affects the heat transfer control behaviour of CLT, the working fluid should be re-charged to remove excessive NCG.

Acknowledgments

The study was sponsored by the National Science Foundation of China (NSFC 51476159, 51761145109, 51776193), Dongguan Innovative Research Team Program (2014607101008), the International Science and Technology Cooperation Project of Science and Technology Department of Anhui Province (BJ2090130038), and the Fundamental Research Funds for the Central Universities (WK6030000066).

Nomenclature

C	specific heat capacity [J kg^{-1} °C^{-1}]
M	mass [kg]
P	pressure [kPa]
ΔP	pressure difference between the evaporator and condenser [kPa]
Q	heat transfer rate [W]
T	temperature [°C]
ΔT	temperature difference between the inlet and outlet R134a in the evaporator [°C]
V	volume [m^3]
$\dot{V}$	volume flow rate [m^3 s^{-1}]
X	mass ratio in the gas region of CLT [%]

Greek letters

ρ	density [kg m^{-3}]

Subscripts

CLT	controllable loop thermosyphon
c	condenser of CLT
e	evaporator of CLT
g	glycol solution
GR	gas part of R134a
in	inlet
NCG	non-condensable gas
out	outlet
w	water

References

[1] Reay D., McGlen R., Kew P., 2013. Heat pipes, 6th ed. Butterworth-Heinemann.

[2] Jafari D., Franco A., Filippeschi S., Marco P.D., Two-phase closed thermosyphons: A review of studies and solar applications, Renewable and Sustainable Energy Reviews 53 (2016) 575-593.

[3] Ersöz M.A., Yıldız A., Thermoeconomic analysis of thermosyphon heat pipes, Renewable and Sustainable Energy Reviews 58 (2016) 666-673.

[4] Ling J., Cao Y., Closed-form analytical solutions for radially rotating miniature high-temperature heat pipes including non-condensable gas effects, International Journal of Heat and Mass Transfer 43 (2000) 3661-3671.

[5] No H.C., Park H.S., Non-iterative condensation modeling for steam condensation with non-condensable gas in a vertical tube, International Journal of Heat and Mass Transfer 45 (2002) 845-854.

[6] Rao V.D., Krishna V. M., Sharma K.V., Rao P.V.J. M., Convective condensation of vapour in the presence of a non-condensable gas of high concentration in laminar flow in a vertical pipe, International Journal of Heat and Mass Transfer 51 (2008) 6090–6101.

[7] Prado-Montes P., Mishkinis D., Kulakov A., Torres A., Pérez-Grande L., Effects of non-condensable gas in an ammonia loop heat pipe operating up to 125 °C, Applied Thermal Engineering 66 (2014) 474-484.

[8] Senjaya R., Inoue T., Effects of non-condensable gas on the performance of oscillating heat pipe, part I: Theoretical study, Applied Thermal Engineering 73 (2014) 1387-1392.

[9] Senjaya R., Inoue T., Effects of non-condensable gas on the performance of oscillating heat pipe, part II: Experimental study, Applied Thermal Engineering 73 (2014) 1393-1400.

[10] He J., Miao J., Bai L., Lin G, Zhang H., Wen D., Effect of non-condensable gas on the startup of a loop heat pipe, Applied Thermal Engineering 111 (2017) 1507-1516.

[11] Yang R., Lin G., He J., Bai L., Miao J., Investigation on the effect of thermoelectric cooler on

LHP operation with non-condensable gas, Applied Thermal Engineering 110 (2017) 1189-1199.

[12] Mantelli M.B.H., Ângelo W.B., Borges T., Performance of naphthalene thermosyphons with non-condensable gases – Theoretical study and comparison with data, International Journal of Heat and Mass Transfer 53 (2010) 3414–3428.

[13] Singh R., Akbarzadeh A., Mochizuki M., Operational characteristics of the miniature loop heat pipe with non-condensable gases. International Journal of Heat and Mass Transfer 53 (2010) 3471–3482.

[14] Huang J., Zhang J., Wang L., Review of vapour condensation heat and mass transfer in the presence of non-condensable gas, Applied Thermal Engineering 89 (2015) 469-484.

[15] Launay S., Sartre V., Bonjour J., Parametric analysis of loop heat pipe operation: a literature review. International Journal of Thermal Sciences 46 (2007) 621–636.

[16] Tong Z., Liu X., Jiang Y., Experimental study of the self-regulating performance of an R744 two-phase thermosyphon loop, Applied Energy 186 (2017) 1–12.

[17] Ziapour B.M., Khalili M.B., PVT type of the two-phase loop mini tube thermosyphon solar water heater, Energy Conversion and Management 129 (2016) 54–61.

[18] Mameli M., Mangini D., Vanoli G.F.T., Araneo L., Filippeschi S., Marengo M., Advanced multi-evaporator loop thermosyphon, Energy 112 (2016) 562-573.

[19] Zhang L., Hua M., Zhang X., Visualized investigation of gas–liquid stratified flow boiling of water in a natural circulation thermosyphon loop with horizontal arranged evaporator, International Journal of Heat and Mass Transfer 102 (2016) 980–990.

[20] Panse S.S., Kandlikar S.G., A thermosiphon loop for high heat flux removal using flow boiling of ethanol in OMM with taper, International Journal of Heat and Mass Transfer 106 (2017) 546–557

[21] Louahlia-Gualous H., Masson S.L., Chahed A., An experimental study of evaporation and condensation heat transfer coefficients for looped thermosyphon, Applied Thermal Engineering

110 (2017) 931–940.

[22] Zhang H., Shi Z., Liu K., Experimental and numerical investigation on a CO_2 loop thermosyphon for free cooling of data centers, Applied Thermal Engineering 111 (2017) 1083–1090.

[23] Dube V., Akbarzade A., Andrews J., The effects of non-condensable gases on the performance of loop thermosyphon heat exchangers, Applied Thermal Engineering 24 (2004) 2439–2451.

[24] Toyoda H., Nakajima T., Kondo Y., Idei A. Sato S., A design for loop thermosyphon including effect of non-condensable gas, 8th ASME/JSME Thermal Engineering Joint Conference, American Society of Mechanical Engineers, 2011.

[25] He J., Lin G., Bai L., Miao J., Zhang H., Wang L., Effect of non-condensable gas on startup of a loop thermosyphon, International Journal of Thermal Sciences 72 (2013) 184-194.

[26] He J., Lin G., Bai L., Miao J., Zhang H., Wang L., Effect of non-condensable gas on steady-state operation of a loop thermosyphon, International Journal of Thermal Sciences 81 (2014) 59-67.

[27] Huang J., Wang L., Shen J., Liu C., Effect of non-condensable gas on the start-up of a gravity loop thermosyphon with gas–liquid separator, Experimental Thermal and Fluid Science 72 (2016) 161-170.

[28] Battaglia F., Singer F., Dessiatoun S.V., Ohadi M.M., Comparison of near source two-phase flow cooling of power electronics in thermosiphon and forced convection modes, Thermal and Thermomechanical Phenomena in Electronic Systems (ITherm), 16th IEEE Intersociety Conference, IEEE, 2017.

[29] Cao J., Pei G., Chen C., Jiao D., li J., Preliminary study on variable conductance loop thermosyphons, Energy Conversion and Management 147 (2017) 66–74

[30] Cao J., Li J., Zhao P., Jiao D., Li P., Hu M., Pei G., Performance Evaluation of Controllable Separate Heat Pipes, Applied Thermal Engineering 100 (2016) 518-527

[31] Cao J., Pei G., Jiao D., Zhao P., Li J., Wang Y., Experimental investigation on controllable loop

thermosyphon with a reservoir, Applied Thermal Engineering 126 (2017) 322-329

[32] Ji J., He H., Chow T., Pei G., He W., Liu K., Distributed dynamic modeling and experimental study of PV evaporator in a PV/T solar-assisted heat pump, International Journal of Heat and Mass Transfer 52 (2009) 1365-1373.

[33] Cheng W., Ding M., Yuan X., Han B., Analysis of energy saving performance for household refrigerator with thermal storage of condenser and evaporator, Energy Conversion and Management 132 (2017) 180-188.

[34] Elarem R., Mellouli S., Abhilash E., Jemni A., Performance analysis of a household refrigerator integrating a PCM heat exchanger, Applied Thermal Engineering 125 (2017) 1320-1333.

[35] Liu Z., Zhao F., Zhang L., Zhang R., Yuan M., Chi Y., Performance of bypass cycle defrosting system using compressor casing thermal storage for air-cooled household refrigerators, Applied Thermal Engineering 130 (2018) 1215–1223.

Figure Captions

Table captions

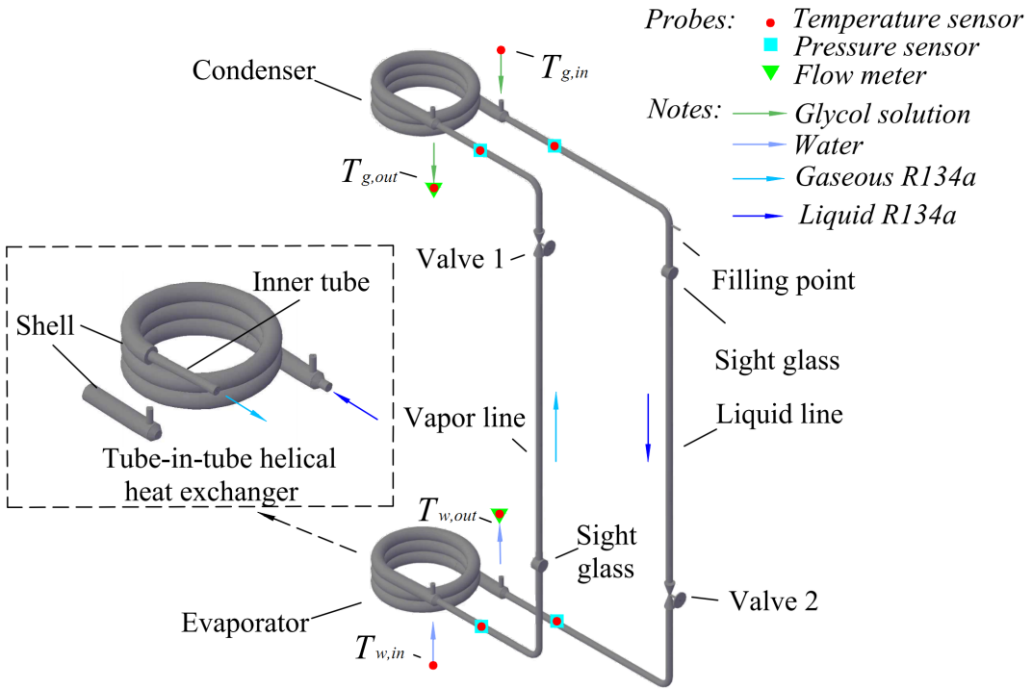

Fig. 1. Layout of the CLT structure and measurement points.

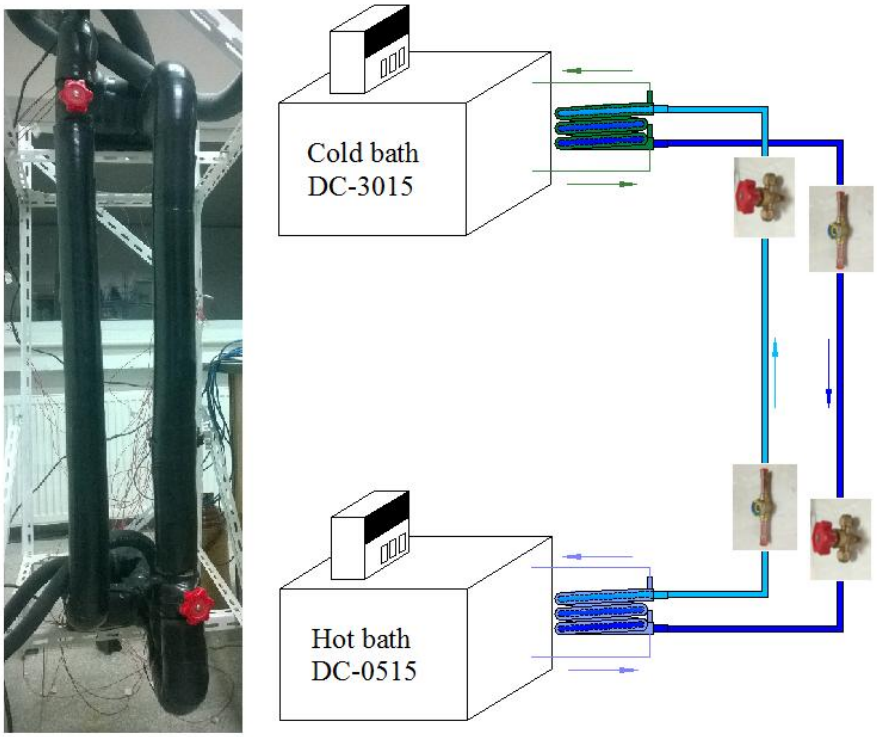

Fig. 2. Experimental platform.

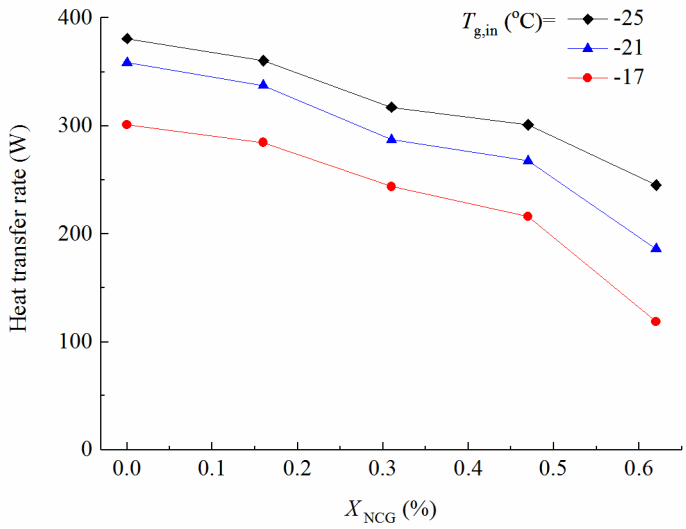

Fig. 3. Heat transfer rates versus X_{NCG} for different $T_{g,in}$.

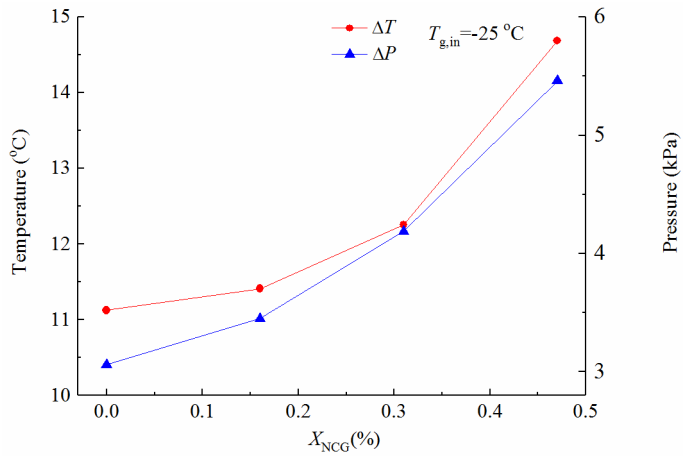

Fig. 4. ΔT and ΔP versus X_{NCG} when $T_{g,in}$ is −25 °C.

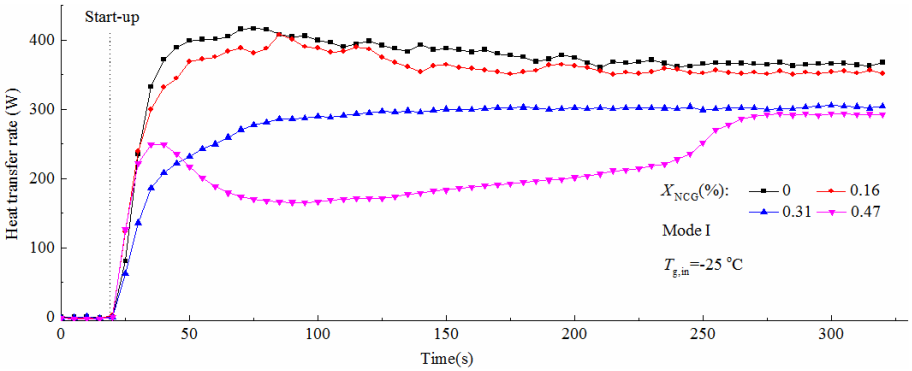

Fig. 5. Start-up behaviours of mode I for different X_{NCG} when $T_{g,in}$ is −25 °C.

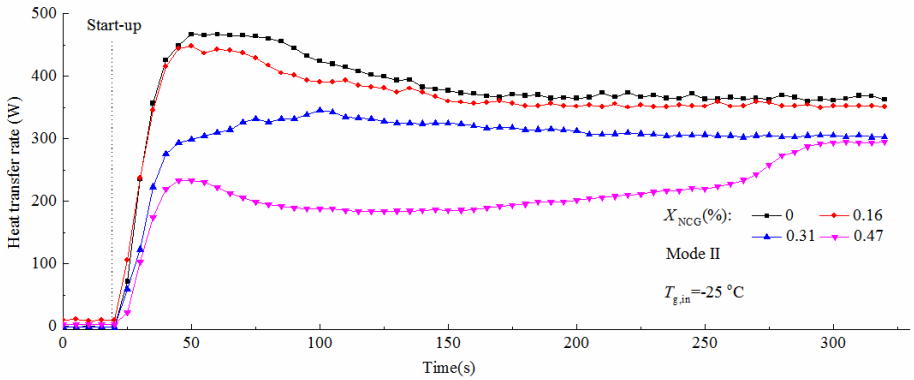

Fig. 6. Start-up behaviours of mode II for different X_{NCG} when $T_{g,in}$ is −25 °C.

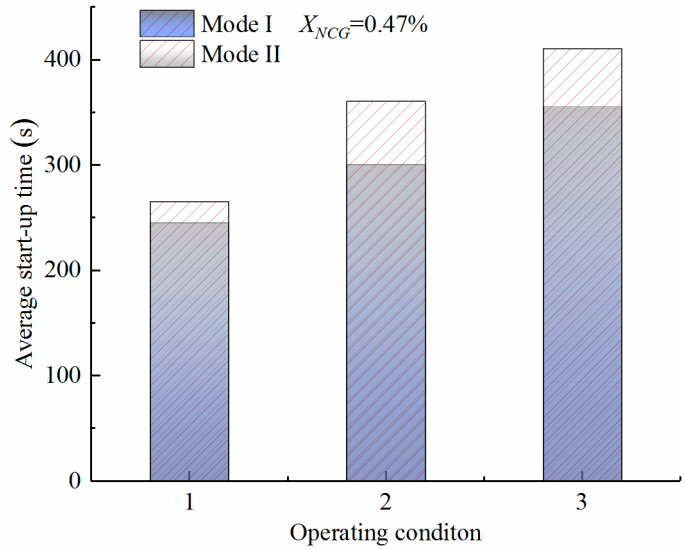

Fig. 7. Average start-up time of CLT with 0.47% NCG for different control modes and operating conditions.

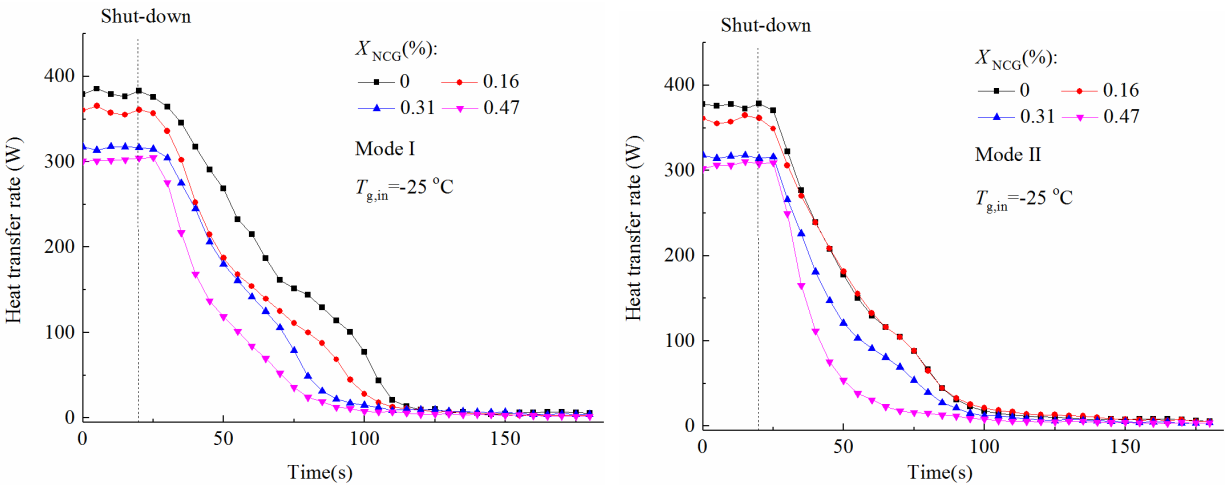

(a) Mode I (b) Mode II

Fig. 8. Stopping procedures of CLT for different X_{NCG} when $T_{g,in}$ is −25 °C.

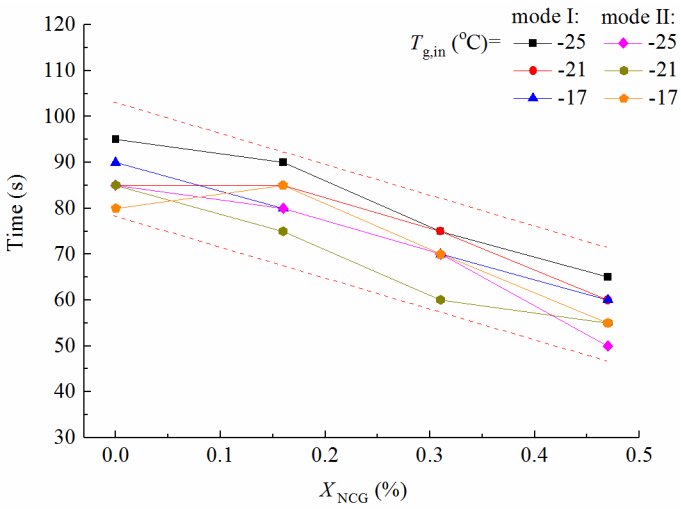

Fig. 9. Stopping time of modes I and II for different X_{NCG}.

Table 1. Measurement devices

Device	Specification	Range	Accuracy
Pressure sensor	JT-131	0 kPa-1000 kPa	0.5%
Temperature sensor	WZP-291 Pt100	–40 °C-100 °C	±0.1 °C
Flow meter	Glass rotameter	16 L/h-160 L/h	2.5%
Electronic balance	KFS-C1	0 kg-1 kg	±0.5 g

Table 2. Average start-up time for different X_{NCG} and $T_{g,in}$

Mode	X_{NCG} (%)	$T_{g,in}$ (°C)				
		−25	−23	−21	−19	−17
I	0	20 s	20 s	20 s	25 s	25 s
	0.16	25 s	25 s	15 s	20 s	25 s
	0.31	35 s	65 s	250 s	460 s	880 s
	0.47	245 s	400 s	850 s	1130 s	\
II	0	20 s	20 s	25 s	20 s	25 s
	0.16	20 s	20 s	15 s	30 s	30 s
	0.31	55 s	150 s	260 s	480 s	920 s
	0.47	265 s	700 s	1180 s	1300 s	\

Highlights

1. A controllable loop thermosyphon (CLT) with non-condensable gas (NCG) is designed.
2. The start-stop performance of CLT is experimentally investigated.
3. While NCG ratio is less than 0.16%, the start-up time remains stable within 15-30 s.
4. The heat transfer and start-up behaviors significantly reduce while the NCG ratio reaches 0.47%.